Beyond 20% World Record Efficiency for Thin-Film Solar Modules

Hossam Elanzeery, Marko Stölzel, Patrick Eraerds, Peter Borowski, Hisham Aboulfadl, Alberto Lomuscio, Detlef Helmecke, Christian Schubbert, Souhaib Oueslati, Matej Hála, Julian Röder, Florian Giesl, and Thomas Dalibor, *Member, IEEE*

***Abstract*—We report on crossing the 20% efficiency line for thin-film solar modules. The efficiency of our cadmium-free Cu(In,Ga)(S,Se)$_2$ (CIGSSe) mid-sized modules (30 × 30 cm^2) based on the cost-efficient AVANCIS stacked elemental layer – rapid thermal processing absorber process has evolved in the last two years reaching 19.6%, 19.8% and recently we have achieved an efficiency level of 20.3% as independently measured by NREL. The recent improvements were made possible by thorough variations in absorber composition and elemental distribution. The optimization of the absorber thickness, and of the band gap profile through the engineering of sulfur content and gradient at the absorber surface induces an improved absorber quality leading to a distinct increase in the product of short circuit current density and open circuit voltage ($J_{SC} \times V_{OC}$). Moreover, improving the absorber homogeneity and adjusting the absorber-buffer interface play an important role in enhancing the fill factor.**

***Index Terms*—CIGSSe, photovoltaic modules, record efficiency, solar modules, thin-film.**

I. Introduction

SOLAR energy is a clean, free, and sustainable energy source. Thin-film technology is considered the second generation for photovoltaic modules. The most potential thin-film technologies from the point of view of cost-efficient and stable efficiency can be limited to Cadmium Telluride (CdTe) and Cu(In,Ga)(S,Se)$_2$ or (CIGS). The CIGS compound is a thin-film technology based on CuIn(S,Se)$_2$ (CIS) and CuGa(S,Se)$_2$ (CGS) [1], with a band gap that can be varied from around 1.0 eV (CIS) to around 2.4 eV (CGS) [2]. On cell-scale, CdTe has reached an efficiency of 22.3% whereas CIGS has achieved 23.6% [3]. For module scale, CdTe has reached a maximum efficiency of 19.5% for a full-size module, whereas for CIGS, AVANCIS raised the record efficiency within the last two years achieving efficiencies of 19.6% and 19.8% on 30 × 30 cm^2 module-size [3]. In this publication, we report on the path to achieve a record efficiency for mid-sized modules of 20.3% as the highest ever reported light-to-electricity conversion of cost-efficient thin-film photovoltaic technologies and being the first thin-film technology to break the 20% efficiency line on a module level of size 30 × 30 cm^2.

Manuscript received 26 September 2023; revised 12 October 2023; accepted 15 October 2023. Date of publication 30 October 2023; date of current version 18 December 2023. *(Corresponding author: Hossam Elanzeery.)*

The authors are with AVANCIS GmbH, 81739 Munich, Germany (e-mail: hossam.elanzeery@gmail.com; marko.stoelzel@avancis.de; patrick.eraerds@avancis.de; peter.borowski@avancis.de; hisham.aboulfadl@avancis.de; alberto.lomuscio@avancis.de; detlef.helmecke@avancis.de; christian.schubbert@avancis.de; souhaib.oueslati@avancis.de; matej.hala@avancis.de; julian.roeder@avancis.de; florian.giesl@avancis.de; thomas.dalibor@avancis.de).

Color versions of one or more figures in this article are available at https://doi.org/10.1109/JPHOTOV.2023.3326559.

Digital Object Identifier 10.1109/JPHOTOV.2023.3326559

II. Module Formation and Characterization

The presented breakthrough was achieved at the Munich R&D research center dedicating a complete pilot line for the production of 30 × 30 cm^2 modules. An overview of our pilot line process is presented in Fig. 1.

A. Absorber Formation

A higher strain point soda lime float glass is used as the substrate. A Silicon Nitride (SiN) layer is then deposited to act as an alkali diffusion barrier. A double layer of Molybdenum (Mo) metal with a Selenium (Se) barrier layer in between is deposited on top of the SiN [4]. A first patterning step is performed to define the cell structure using a picosecond (ps) laser process.

Afterward, a low-temperature precursor deposition is performed using the proprietary so-called stacked elemental layer (SEL) process where a sodium-doped copper-indium-gallium (Cu-In-Ga:Na) precursor layer is deposited using magnetron sputtering followed by a Se capping layer deposited by thermal evaporation [5]. The absorber formation is then completed by annealing the precursor stack using a rapid thermal processing (RTP) tool in a sulfur-containing atmosphere leading to the formation of the CIGSSe absorber semiconductor.

B. Heterojunction Layers and Patterning

After the absorber formation, a Na-based postdeposition-treatment (PDT) step is introduced to passivate and enhance the absorber surface and bulk. The Na concentration and annealing temperature were adapted in order to achieve an optimized module efficiency. No heavy alkali PDT is used in the experiments and modules reported in this article. Then, a sputtered zinc-oxysulfide Zn(O,S) buffer layer [6], [7] is deposited on top of the treated absorber surface.

The second patterning step is conducted using a ps laser process before the deposition of an aluminum-doped zinc-oxide (ZnO:Al) window layer using magnetron sputtering. The final patterning step is performed by a mechanical scribing technique achieving a dead zone down to 60 μm.

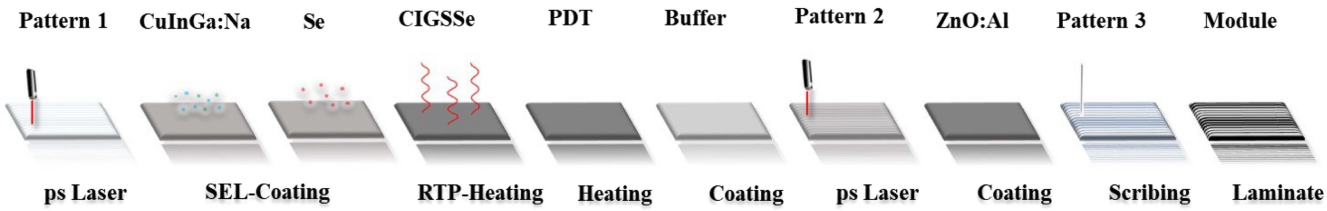

Fig. 1. AVANCIS standard pilot line process.

C. Module Formation

The module is then contacted and encapsulated with a lamination foil and front glass with antireflective properties.

D. Characterization

Different characterization techniques are applied at different stages of the module formation. Characterization techniques from #1 to #6 were performed on bare absorbers after completing the RTP step, while characterization techniques #7 and #8 were performed on complete-stack modules. Detailed description of each characterization technique is described as follows.

1) Optical Scanner: A Microtek ScanMaker 9800XLPlus is used to obtain a scanned image of the absorber front surface after the RTP step using CCD technology.

2) Time-Resolved Photoluminescence: A pulsed diode laser with a wavelength of 638 nm and pulse width of about 200 ps is used to excite the absorber. The emitted signal is detected by a germanium avalanche photodiode cooled down with liquid nitrogen; the system is equipped with a band pass filter (715 nm) to block the excitation laser signal. For each sample, multiple measurements are performed on different spots to check the homogeneity and to get a representative value indicating the lifetime of the whole absorber.

3) Glow-Discharge-Optical-Emission-Spectroscopy (GDOES): Depth profile analysis by GDOES was applied to evaluate the chemical composition within the CIGSSe absorbers. The system uses an argon plasma for sputtering and a CCD-array to detect the photons emitted during the relaxation of the sputtered and excited atoms and ions in the plasma. All GDOES depth profiles were measured using a GDA 650 HR, a system built by Spectruma Analytik in dc excitation mode (constant voltage – constant current mode) including an anode with an inner diameter of 2.5 mm. The excitation parameters were set to 1000 V and 12 mA. The WinGDOES software was applied to automatically determine quantitative depth profiles of mass concentration which are then corrected with a calibration method developed internally based on [8].

4) Raman Spectroscopy: A HeNe laser is used as an excitation source with a wavelength of 633 nm. For all measurements, the same acquisition parameters were used, i.e., neutral filter, grating, slit width, objective, and monochromator. For each absorber, 9 different spots are measured, with a relative distance of about 50 μm and for each spot 2 acquisitions are carried out. The S/Se values refer to the ratios of the integrated areas of the A1 mode-peaks (S-S and Se-Se, respectively)

5) X-Ray Fluorescence (XRF): XRF measurements were carried out in an S8 Tiger Series-2 Bruker-AXS instrument with a 3 kW-Generator, a scintillation counter and proportional counter. The absorbers were measured under vacuum with 60 kV/50 mA settings using "ML-Quant" software (thin-film program) calibrated with CIGSSe deposited on Mo-Glass.

6) Focused Ion Beam Combined With Transmission Electron Microscopy and Energy Dispersive X-Ray Spectroscopy (FIB-TEM/EDX): These measurements were performed on absorbers using a Dual FIB/SEM (Scanning Electron Microscopy) Zeiss NVision 40 (Carl Zeiss Microscopy GmbH) with dual FIB/SEM FEI Versa 3D (FEI Thermo Fisher) using a FEI Titan3G and SuperX Si-drift EDX detector system.

7) Current-Voltage (I-V): In the AVANCIS' pilot line, I-V parameters are measured at several stages during module production and stabilization: before encapsulation, after encapsulation, and for the final module, mainly after light-soaking, partially under varying conditions and with varying durations (from hours to several days). High precision I-V measurements are conducted under continuous light with I-V sweeping durations in the range of hundreds of milliseconds. Particular attention is given to temperature control of the device under test during this prolonged exposure to standard test conditions (STC) irradiation. As a light source, a Xenon light bulb is used, calibrated such that a reference device with similar spectral response delivers a short-circuit current (I_{SC}) as certified by an external lab under STC. Short-pulsed measurements (flasher) are conducted for verification.

For monolithically interconnected thin-film modules, the definition of the correct aperture as required by certifying labs can be crucial. Although the aperture is clearly defined by the laser scribes of the cell structuring and the isolation cuts perpendicular, for external measurements, we additionally apply an opaque frame onto the front glass. Depending on the geometry of the simulator's light source and the sample as well as the ratio of diffuse and direct light, the shadow cast by the opaque frame differs and can lower the irradiance on the first and the last cell in the serial connection, leading to differing measured I-V curves depending on the detailed setup of the sun simulator.

8) External Quantum Efficiency (EQE): For measurement of the quantum efficiencies or spectral response, an individual cell is electrically contacted during production of the thin-film module. The EQE is then measured on the encapsulated device using monochromatic chopped light together with a white bias light. Spatial homogeneity of spectral response has been

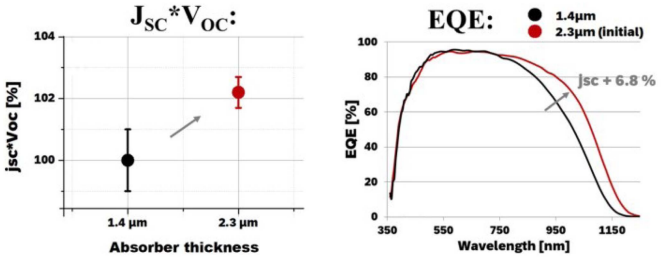

(a) (b)

Fig. 2. (a) $J_{SC} \times V_{OC}$ as a function of absorber thickness. (b) EQE curve for two different absorber thicknesses indicates the increase in J_{SC} with increasing absorber thickness.

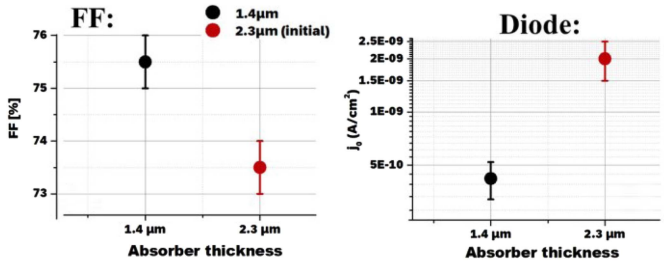

(a) (b)

Fig. 3. (a) FF values and (b) saturation current density (J_0) for the two absorber thicknesses indicating worsened diode parameters with increasing absorber thickness.

quantified for individual samples but cannot be guaranteed for all devices produced. Together with routine measurements of the spectral distribution of the sun simulator, spectral mismatch factors are computed but turn out to be negligible for most devices, considering the measurement errors inherent to both the EQE and spectral measurements.

III. Route Toward 20%

The achieved record efficiencies are based on a route of optimizations for different process steps. Coming from a 16.6% module record efficiency in 2014 up to an efficiency of 19% in 2019 [9], the optimizations were first focused on having a Cd-free buffer layer by introducing a Na-doped InS buffer with either an intrinsic ZnO layer or later with an intrinsic (Zn,Mg)O layer (achieving an efficiency milestone of 18 %) [10].

Afterward, the Na-doped InS buffer and intrinsic (Zn,Mg)O layers were replaced with a Na-PDT step followed by a Zn(O,S) buffer layer, which allows process simplification in terms of direct sputtering of the ZnO:Al window layer atop of Zn(O,S) buffer layer [7], [9], [10]. Finally, the main focus was shifted toward optimizing the absorber quality with consequent Na-PDT and Zn(O,S) buffer adjustments as summarized in the following sections.

A. Absorber Thickness

The CIGS absorber thickness was increased from 1.4 to 2.3 μm leading to an increase in the Current-Voltage product, short circuit current density × open circuit voltage, ($J_{SC} \times V_{OC}$) as illustrated in Fig. 2(a). This increase in $J_{SC} \times V_{OC}$ is affected mainly by the increase of J_{SC} due to increased absorption as a result of the thicker part of the absorber layer [11]. This can be derived from the long wavelength region in the EQE of Fig. 2(b).

Although the increase in $J_{SC} \times V_{OC}$ product was quite significant after increasing the absorber thickness, the fill factor (FF) could not be maintained for the initial thicker absorber type due to inferior diode parameters as depicted in Fig. 3 (both saturation current density J_0, and ideality factor n, showed worse values, but only J_0 is presented here), leading to a slight reduction in the total efficiency.

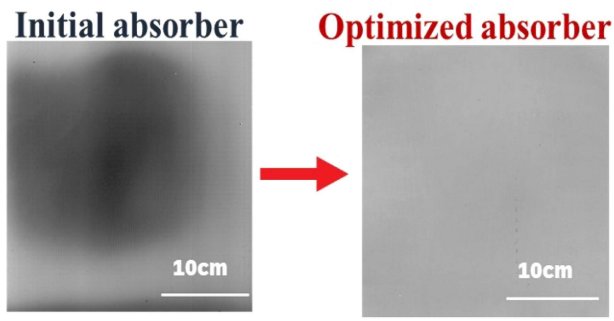

Fig. 4. Optical scanned image of the thick absorber type before and after optimization.

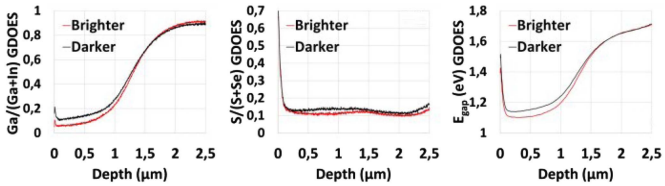

(a) (b) (c)

Fig. 5. GDOES profiles of (a) [Ga]/([Ga]+[In]) ratio, (b) [S]/([S]+[Se]) ratio, and (c) band gap (E_{gap}) of darker and brighter appearing areas within the same 30 × 30 cm^2 absorber.

B. Absorber Homogeneity

Deeper analysis of the thicker absorber type revealed a strong inhomogeneity within the same absorber material with areas showing a darker appearance compared with surrounding brighter appearance areas as illustrated in Fig. 4.

The analyses of the darker and brighter appearing areas revealed that the darker area is characterized by a higher roughness, higher Ga toward the absorber surface, higher S at the absorber bulk, and consequently higher bandgap (E_{gap}) as shown by the GDOES profiles in Fig. 5.

Several optimization steps were performed to improve the absorber homogeneity. A more homogeneous absorber appearance could be achieved by varying the chalcogens during the absorber formation through the following two approaches.

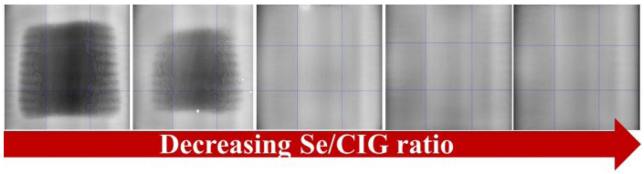

Fig. 6. Optical scanned images for absorber appearance as a function of varying the Se/CIG ratio.

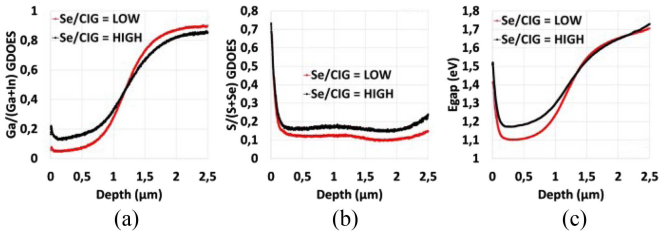

Fig. 7. GDOES profiles of (a) [Ga]/([Ga]+[In]) ratio, (b) [S]/([S]+[Se]) ratio, and (c) band gap (E_{gap}) of two different absorbers with low and high Se/CIG ratio.

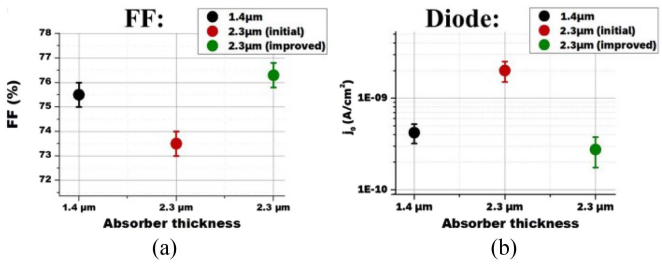

Fig. 8. (a) FF values and (b) saturation current density (J_0) for a thin absorber type of 1.4 μm (black), an un-optimized thick absorber type of 2.3 μm (red) and an optimized thick absorber type (green).

1) The Se/Metal ratio (Se/CIG ratio) was optimized within the precursor. Decreasing the Se/CIG ratio helps to improve the absorber homogeneity as observed in Fig. 6 as an effect of reducing Ga toward the absorber front surface and consequently reducing the absorber front band gap (enhancing the FF values) as confirmed by the GDOES profiles of low and high Se/CIG ratios in Fig. 7.
2) The sulfur profile was optimized within the absorber formation as will be explained in more detail in the following subsection.

These optimizations for the absorber homogeneity resulted in significant improvement in the absorber appearance as shown in Fig. 4 as well as an enhancement in FF and diode parameters as presented in Fig. 8 and published in [11] and [12].

On the other side, reducing the Se/CIG ratio leads to slight reduction of S in the absorber bulk depicted in Fig. 7 which leads to a reduction of the $J_{SC} \times V_{OC}$ product. For the above-mentioned reason, an optimization to successfully combine the advantages of the improved $J_{SC} \times V_{OC}$ product (from increased absorber thickness) and FF (from improved absorber uniformity) was required.

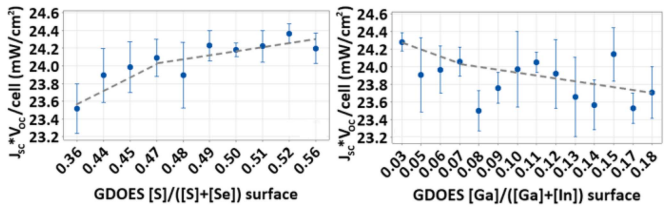

Fig. 9. $J_{SC} \times V_{OC}$ product as a function of (a) [S]/([S]+[Se]) ratio and (b) [Ga]/([Ga]+[In]) ratio at absorber front surface as determined from GDOES profiles.

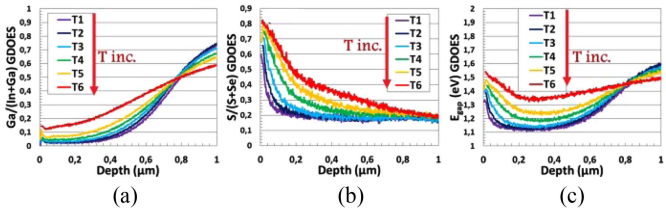

Fig. 10. GDOES profiles of (a) [Ga]/([Ga]+[In]) ratio, (b) [S]/([S]+[Se]) ratio, and (c) band gap (E_{gap}) for a variation of the RTP annealing temperatures above 500 °C.

C. Sulfur Optimization Through the RTP Step

As reported in Section III-B, reducing the Se/CIG ratio succeeded in enhancing the homogeneity (and FF) of the thick absorber type in exchange of losses in the $J_{SC} \times V_{OC}$ product. The RTP step was then optimized with the goal of improving the band alignment between the absorber and buffer layers. This was achieved by optimizing the ratios of [S]/([S]+[Se]) from the absorber front surface with the [S]/([S]+[O]) ratio of the Zn(O,S) buffer layer, which resulted in improving the $J_{SC} \times V_{OC}$ product without negatively affecting the absorber homogeneity.

Our thorough analysis shows that the optimization is mostly governed by the valence band and not by the pure surface band gap widening of the absorber surface as can be derived from Fig. 9. The $J_{SC} \times V_{OC}$ product improves with increasing the [S]/([S]+[Se]) ratio and not by increasing the [Ga]/([Ga]+[In]) ratio at the absorber front surface despite the fact that both ratios will lead to widened absorber surface band gaps when increased. While the Ga surface increase mainly acts on the conduction band, the S surface increase leads to both a lowered valence band and an increased conduction band [13].

Optimizing the RTP step plays an important role for optimizing the S in the absorber bulk and toward the absorber front surface without significantly varying the Ga toward the absorber front surface, as illustrated in Fig. 10.

According to Fig. 10, increasing the RTP annealing temperature (above 500 °C) promotes more incorporated S toward the absorber bulk and absorber front surface leading to an increase in the bandgap (with a corresponding increase in V_{OC} for optimized absorbers) without increasing Ga significantly toward the absorber surface (except for very high temperatures). The RTP annealing temperature was optimized to be low enough to have

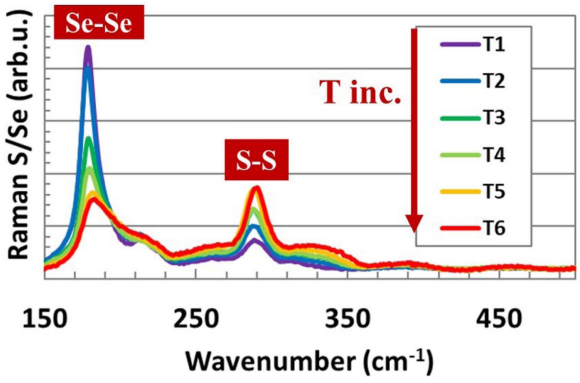

Fig. 11. Raman spectra for varying RTP annealing temperature above 500 °C.

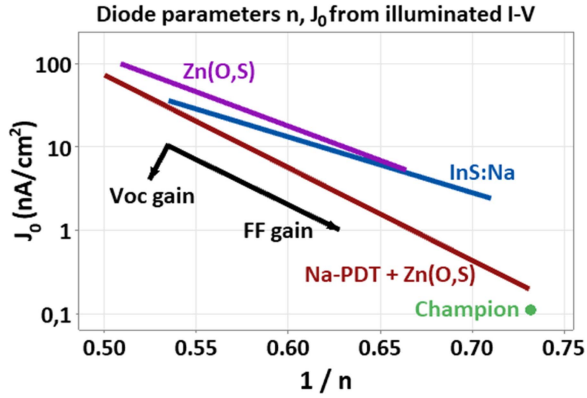

Fig. 12. Correlation between saturation current density (J_0) and ideality factor (n) for the effect of Na on different buffer layers. The three lines represent linear fits from experimental data.

minimal effect on the Ga-profile, while achieving the desired increase in S (and corresponding V_{OC} increase). This observation can also be supported by the Raman measurements. Raman spectra plotted as a function of RTP annealing temperature reveal that a rise in the temperature results in the exchange of the Se-compound by the S-compound where more active S atoms are incorporated. This can be observed from the intensity reduction of the Se-compound compared with the intensity increase of the S-compound as shown in the A1 modes of Fig. 11. The lines at 180 and 290 cm^{-1} are attributed to Se-Se and S-S vibrations, respectively.

Moreover, the RTP step is optimized to avoid the increase of S toward the absorber backside. An increased S-incorporation toward the $Mo(S,Se)_2$ layer has been proven to be the root cause of a secondary barrier at the back interface for high sulfurization levels [14], [15].

The recent improvements were achieved by optimizing the band gap profile through the engineering of sulfur content and gradient, especially at the absorber surface which induced an improved absorber quality (improved carrier lifetime) with a distinct increase in J_{SC}.

D. PDT and Buffer Optimizations

A sputtered Zn(O,S) buffer is already the second generation of Cd-free dry buffers processed by physical vapor deposition (PVD) at AVANCIS. The first generation Cd-free buffer was an In_xS_y-based buffer layer, instead of the classical chemical bath deposited (CBD) CdS buffer [4]. A dry PVD process prevents the costly and harmful wastewater disposal, such as required in the case of CBD of CdS or Zn(O,OH)S buffers, and In_xS_y improves optical response in comparison to CdS.

However, also evaporated In_xS_y buffer imposed certain limitations, such as inferior blue response with respect to Zn(O,S), as well as the relative complexity of the evaporation process with respect to sputtering using a scalable Zn(O,S) target.

In the case of sputtered Zn(O,S) buffer, a careful adjustment of its [S]/([S]+[O]) ratio as well as tuning of Na-PDT in terms of alkali distribution within absorber-buffer interface was found essential to enhance diode behavior, which in turn enabled the high efficiency levels for the R&D modules. It was observed, that Na-PDT drives significant V_{OC} and FF improvements by reducing nonradiative recombination losses experienced with Zn(O,S) buffer, as depicted in Fig. 12. The lines in Fig. 12 are linear fits from experimental data.

TABLE I
EXTERNALLY CERTIFIED I-V CHARACTERISTICS

Efficiency (%)	V_{OC} (mV)/cell	J_{SC} (mA/cm^2)	FF (%)
19.6	688.1	37.6	75.9
19.8	687.8	38.0	75.9
20.3	683.4	39.5	75.1

IV. CHAMPION MODULE

Several optimization approaches were presented in this article. AVANCIS latest independently certified world record aperture area efficiency of 20.3% (certified by NREL) for laminated CIGSSe modules of size 30 × 30 cm^2 was achieved by variations in absorber composition and elemental distribution, as well as adjustments in Na-PDT and Zn(O,S) buffer.

Principally, the optimization of the band gap profile through the engineering of both gallium and sulfur contents and their gradients at the absorber surface induces an improved absorber quality and distinct increase in J_{SC} at nearly no losses in V_{OC}. The improvement in $J_{SC} \times V_{OC}$ product is then the main contributor to the achievement of an overall higher efficiency of 20.3%, despite small losses in FF as compared with the previous 19.8% champion module (likewise certified by NREL). In this section, we will present the main characteristics of our recent champion module.

Fig. 13 presents the data of the I-V measurement at NREL of our 30 × 30 cm^2 champion module (measured under a continuous light solar simulator). The module was stabilized by light-soaking prior to measurement.

In Fig. 14, we depict the long track record of champion efficiencies of AVANCIS' 30 × 30 cm^2 R&D CIGSSe modules.

Table I provides the primary I-V characteristics of AVANCIS' latest three record module efficiencies as externally certified by NREL.

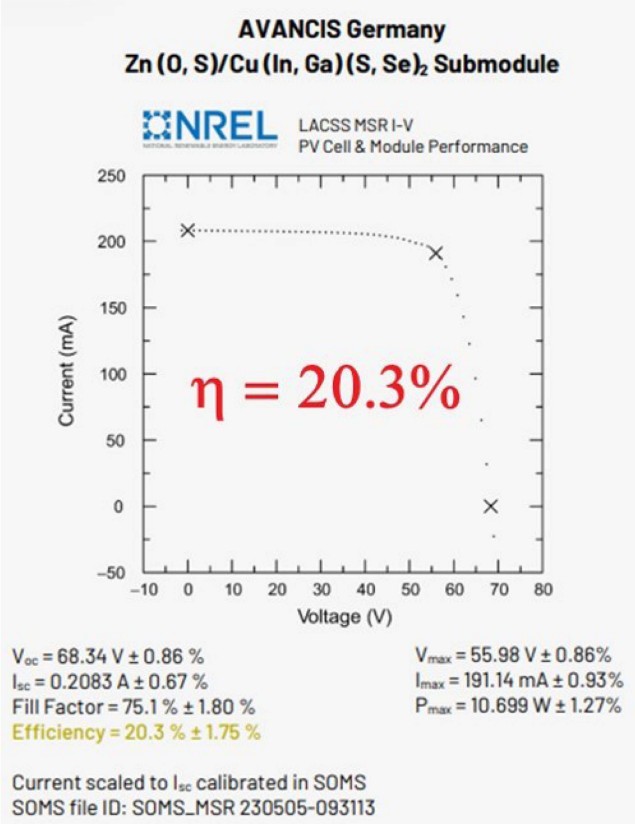

Fig. 13. I-V curve of the certification measurement at NREL.

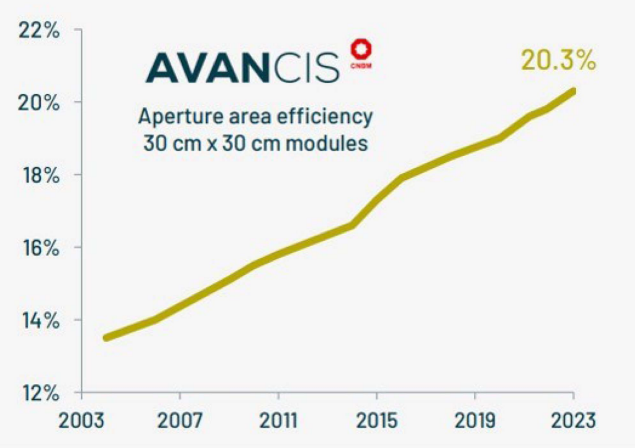

Fig. 14. Evolution of AVANCIS' 30 × 30 cm^2 externally certified champion module efficiencies.

Different characterization techniques were used to investigate the improvements achieved in our recent record process (measured on absorber types similar to the ones used for our champion module) compared with our previous record.

Fig. 15(a) illustrates the Raman and XRF (inset) measurements for S of two absorber types: the absorber of our recent champion module with red points, and the absorber of our previous champion module with blue points. The sulfur profile

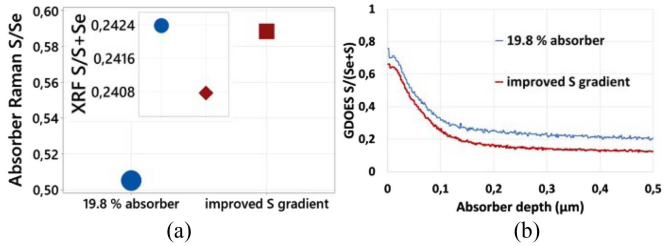

Fig. 15. (a) S/Se ratio from Raman measurements and sulfur to chalcogen ratio from XRF measurements (inset). (b) GDOES [S]/([S]+[Se]) ratio for the two different absorber types; recent record (red) and previous record (blue).

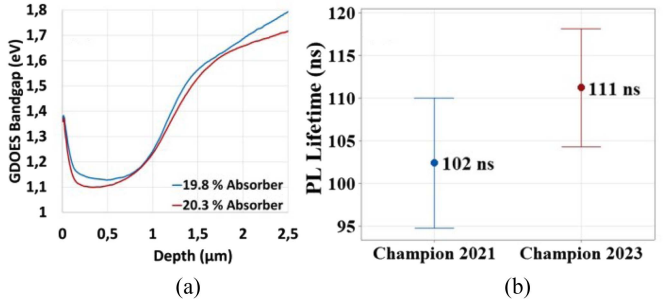

Fig. 16. (a) Band gap (E_{gap}) profile from GDOES measurements and (b) photoluminescence (PL) lifetime for absorbers similar to our recent (red curve) and our previous (blue) record efficiencies.

in the absorber was optimized in a way that the optical active S (Raman) toward the surface was increased despite a slight overall reduction of compositional S in the absorber (XRF data).

The increased Raman S/Se signal shows the strong increase of the active surface-S despite the lower S content at the surface as depicted from the sulfur GDOES profiles in Fig. 15(b) indicating an enhanced incorporation of optical and electrical active S in the absorber crystals and not only elemental S located to the grain boundaries [16], [17].

This optimization process was achieved by controlling the S-incorporation during ramping phases. It was found that a strong dependence of the anion ratio [S]/([S]+[Se]) on the [Cu]/([In]+[Ga]) ratio takes place when S is incorporated during the temperature ramping up phase [5], [18], [19], [20].

On the other side, the Ga-profile was also optimized in order to reduce Ga toward the front surface (first 500 nm) and move it toward the back surface. This change in Ga profile helped to further improve both front and back interface surfaces. Lower Ga toward the absorber front surface helped to improve the band alignment with the buffer layer whereas increasing Ga toward the back surface helped to reduce the diffusion of sulfur toward the back-absorber side in order to prevent the formation of backside interface barriers.

Indeed, reducing Ga toward the absorber front surface (with slight increase of active S at the front surface) succeeded in reducing the band gap minimum in the absorber bulk as can be observed in Fig. 16(a). The reduction in the band gap minimum (based on Ga-reduction) whereas increasing S toward front surface helped to avoid losses in V_{OC}, improving the V_{OC}-deficit

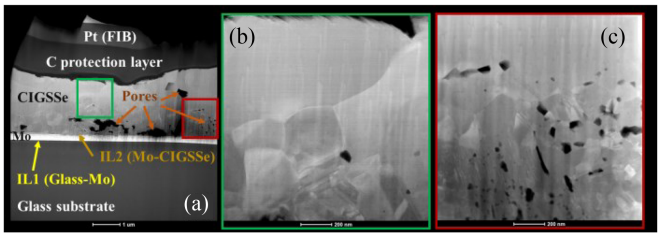

Fig. 17. STEM microstructure for (a) an absorber similar to the absorber of our recent record module, (b) absorber front side [green square in (a)] with large grains indicating high absorber quality, and (c) absorber back side [red square in (a)] with large number of voids indicating relatively poorer absorber quality and potential nonradiative recombination sources. Arrows point out pores. IL1 is the first interface layer between Mo and glass whereas IL2 represents the second interface layer between Mo and absorber back side.

by more than 30 mV and increasing the J_{SC} (as a result of band gap lowering), thus significantly improving the $J_{SC} \times V_{OC}$ product. The enhancement in the V_{OC}-deficit is also supported by the increase of the PL lifetime (about 10 ns in average) for our recent absorber compared with our previous one as depicted in Fig. 16(b). Moreover, the S-reduction toward the absorber back interface with Mo plays a role in reducing interface barriers at the back contact and improves the FF.

SEM/TEM microstructure measurements performed on our recent absorber shown in Fig. 17 reveal fine crystallites at the absorber back interface to the Mo contact and larger crystallites of several 100 nm up to μm range in the upper part of the layer. While the absorber bulk to the front surface shows large grains indicating high absorber quality [Fig. 17(b)], the back side of the absorber shows large number of voids [Fig. 17(c)] with black areas within the CIGSSe absorber layer representing pores and indicating that there is still room for improving our recent absorber through optimizing the absorber back interface. This has also been proven by depth-resolved PL spectroscopy measurements that revealed the backside of our CIGSSe absorbers as a source of nonradiative recombination as published in [21].

STEM-EDX measurements confirm the accumulation of S toward the Mo-absorber back interface and toward the absorber surface as observed in Fig. 18. Fig. 18(a) represents the part of the absorber used for the EDX mapping, whereas Fig. 18(b) and (c) represent the Se and S mapping, respectively. S is enriched mainly at the surface, at grain boundaries, toward the Mo back electrode, and around pores as indicated in Fig. 18(c) and by the red arrows in the S-Se mapping of Fig. 18(d) whereas Se is depleted in these regions [see Fig. 18(b)]. In is enriched in the upper part of the absorber (In-rich phase toward the absorber front surface), whereas Ga is enriched in the lower part of the CIGSSe layer (Ga-rich toward the absorber back side) as can be observed in Fig. 18(e). Cu is distributed mostly homogeneous through the absorber layer [see Fig. 18(f)].

Based on the above-mentioned results, it can be concluded that the presented optimization has indeed succeeded in improving the absorber quality through a significant increase of the $J_{SC} \times V_{OC}$ product. The overall efficiency of the module is therefore driven by a gain in $J_{SC} \times V_{OC}$ despite a small loss in FF (slightly worsened J_0 and n) compared with our previous 19.8% absorber.

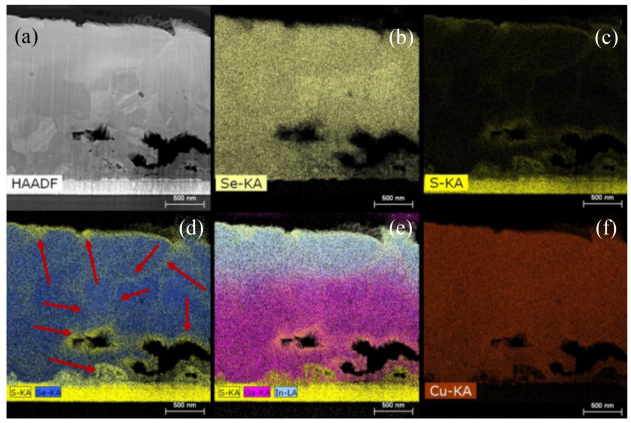

Fig. 18. STEM-EDX mapping for (a) our recent absorber indicating the main elemental distribution: (b) Se, (c) S, and (d) S-Se map showing the distribution of chalcogens through our absorber. (e) S-Ga-In map showing the enrichment of In toward the front surface whereas Ga is enriched toward the back absorber surface. (f) Cu.

V. Conclusion

The presented results demonstrate that the cost-efficient AVANCIS SEL-RTP process combined with an all-sputtered buffer and window layer extends the lead of AVANCIS for thin-film power conversion efficiency. We achieved a new world record aperture area efficiency of 20.3% for monolithically serial connected 30 × 30 cm^2 CIGSSe thin-film PV module (certified by NREL) which is in general the highest value for cost-efficient single junction thin-film PV modules of that size and the first thin-film module in that size to exceed the 20% efficiency line. In addition, these modules do not contain hazardous materials such as lead or cadmium.

Acknowledgment

The authors would like to thank Fraunhofer CSP Institute for performing the FIB-TEM/EDX measurements on our absorbers.

References

[1] H. T. Xue et al., "Phase diagram of the $CuInSe_2$-$CuGaSe_2$ pseudobinary system studied by combined ab initio density functional theory and thermodynamic calculation," *J. Appl. Phys.*, vol. 116, 2014, Art. no. 053512.
[2] M. Turcu, I. M. Kötschau, and U. Rau, "Composition dependence of defect energies and band alignments in the $Cu(In_{1-x}Ga_x)(Se_{1-y}S_y)_2$ alloy system," *J. Appl. Phys.*, vol. 91, pp. 1391–1399, 2002.
[3] Plot is courtesy of the National Renewable Energy Laboratory, Golden, CO, USA, 2023.
[4] J. Palm et al., "Cd-free CIS thin film solar modules at 17% efficiency," in *Proc. 29th Eur. Photovolt. Sol. Energy Conf. Exhib.*, 2014, pp. 1433–1438.
[5] J. Palm, V. Probst, and F. H. Karg, "Second generation CIS solar modules," *Sol. Energy*, vol. 77, pp. 757–765, 2004.
[6] R. Klenk et al., "Sputtered Zn(O,S): A promising approach to dry inline fabrication of Cd-free CIGS modules," in *Proc. IEEE 40th Photovolt. Specialist Conf.*, 2014, pp. 0959–0963.
[7] M. Algasinger et al., "Efficient $Cu(In,Ga)(Se,S)_2$ modules with sputtered Zn(O,S) buffer layer," *Thin Solid Films*, vol. 633, pp. 231–234, 2017.
[8] T. Kodalle et al., "Glow discharge optical emission spectrometry for quantitative depth profiling of CIGS thin-films," *J. Anal. At. Spectrometry*, vol. 34, no. 6, pp. 1233–1241, 2019.
[9] M. Stoelzel et al., "Absorber optimization in CIGSSe modules with a sputtered Zn(O,S) buffer layer at 19% efficiency," in *Proc. 36th Eur. Photovolt. Sol. Energy Conf. Exhib.*, 2019, pp. 590–596, doi: 10.4229/EU-PVSEC20192019-3AO.7.1.

[10] T. Dalibor et al., "Advanced PVD buffers on the road to GW-scale CIGSSe production," in *Proc. IEEE 43rd Photovolt. Specialists Conf.*, 2016, pp. 1433–1437, doi: 10.1109/PVSC.2016.7749853.
[11] P. Eraerds et al., "Improved CIGSSe absorber homogeneity with Cd-free sputtered ZnOS buffer layer at world record efficiency on 30×30 cm^2 laminated module," presented at 38th Eur. Photovolt. Solar Energy Conf. and Exhib., 2021.
[12] M. Stoelzel et al., "Device performance parameter improvements of CIGSSe modules by material optimization," presented at E-MRS, 2021.
[13] S.-H. Wei and A. Zunger, "Band offsets and optical bowings of chalcopyrites and Zn-based II-VI alloys," *J. Appl. Phys.*, vol. 78, no. 6, pp. 3846–3856, 1995.
[14] F. Giesl et al., "Improved modeling of the effect of sulfur on optical and electrical properties in a calibrated simulation model of a CIGSSe solar module," *J. Phys. D Appl. Phys.*, vol. 56, no. 4, Dec. 2022, Art. no. 045105, doi: 10.1088/1361-6463/aca9d9.
[15] F. Giesl et al., "Investigation of electrical transport across the CIGSSe/Mo(Se,S)$_2$ interface of a CIGSSe-based solar cell by experiment and device simulation," *Thin Solid Films*, vol. 763, no. 7, Nov. 2022, Art. no. 139570.
[16] H. Aboulfadl et al., "Microstructural characterization of sulfurization effects in Cu(In,Ga)Se_2 thin film solar cells," *Microsc. Microanalysis*, vol. 25, no. 2, pp. 532–538, 2019, doi: 10.1017/S1431927619000151.
[17] J. Keller et al., "Grain boundary investigations on sulfurized Cu(In,Ga)(S,Se)$_2$ solar cells using atom probe tomography," *Sol. Energy Mater. Sol. Cells*, vol. 117, pp. 592–598, 2013, doi: 10.1016/j.solmat.2013.07.034.
[18] J. Keller et al., "Effect of Cu content on post-sulfurization of Cu(In,Ga)Se_2 films and corresponding solar cell performance," *J. Phys. Status Solidi A*, vol. 216, 2019, Art. no. 1900472, doi: 10.1002/pssa.201900472.
[19] J. Keller et al., "Heavy alkali treatment of post-sulfurized Cu(In,Ga)Se_2 layers: Effect on absorber properties and solar cell performance," *Sol. RRL*, vol. 4, 2020, Art. no. 2000248, doi: 10.1002/solr.202000248.
[20] J. K. Larsen et al., "Sulfurization of co-evaporated Cu(In,Ga)Se_2 as a postdeposition treatment," *IEEE J. Photovolt.*, vol. 8, no. 2, pp. 604–610, Mar. 2018, doi: 10.1109/JPHOTOV.2018.2793759.
[21] A. M. Prot et al., "Composition variations in Cu(In,Ga)(S,Se)$_2$ solar cells: Not a gradient, but an interlaced network of two phases," *APL Mater.*, vol. 11, 2023, Art. no. 101120.

Hossam Elanzeery received the B.Sc. degree in electrical and electronics engineering from the University of Technology Petronas, Malaysia, in 2010, the M.Sc. degree in microelectronics system design from Nile University, Giza, Egypt, in 2014, and the Ph.D. degree in physics from the University of Luxembourg, Esch-sur-Alzette, Luxembourg, in 2019.

As a Manager of New Processes I, he is leading the absorber formation and characterization group with AVANCIS' R&D Center, Munich, Germany. Since 2013, he has been working in thin-film solar cells with more than 40 publications and conference contributions in addition to one book on thin-film solar cells.

Marko Stölzel received the Ph.D. degree in physics from the University of Leipzig, Leipzig, Germany, on photoluminescence of excitons in polar ZnO/MgZnO quantum well structures, in 2014.

After a Postdoctoral position on CuI and ZnO compounds with the University of Leipzig, he joined the AVANCIS R&D Center, Munich, Germany. He is a Manager for New Processes III: patterning, contacting and grid processes on 30 × 30 cm^2. He contributed to 21 reviewed articles, six conference papers as well as a book chapter on semiconductors.

Patrick Eraerds received the Ph.D. degree in physics from the Université de Genève, Geneva, Switzerland, on single photon communication and fiber metrology, in 2010.

In the past years, he led several development projects for CIGS champion efficiencies, leading to certified world records on 30 ×30 cm^2 mini modules. He started his career with AVANCIS, Munich, Germany, on solar cell device simulation followed by process development of evaporated buffer layers and PDT materials. As a Manager, he is heading the group "New Processes II" with the AVANCIS' R&D Center, Munich, Germany.

Peter Borowski received the Ph.D. degree in physics from the Technical University of Dresden, Dresden, Germany, in 2006, for research work on biological physics in sensory cells with the Max-Planck Institute for the Physics of Complex Systems.

After research positions in Germany, Poland, Canada, and India on quantum mechanics and mathematical biology, he entered the world of PV with his employment with AVANCIS, Munich, Germany, where he currently heads the research group for product characterization.

Hisham Aboulfadl received the Ph.D. degree in material science engineering from Saarland University, Saarbrucken, Germany, on diffusion kinetics and phase formation in Ag/Al and Ru/Al multilayer thin-films, in 2017.

Afterward, he worked as a Postdoctoral with Chalmers University, Sweden in a joint-project with Uppsala University focused on development of CIGS thin-film solar cells. He then joined the AVANCIS R&D Center, Munich, Germany, as an R&D Engineer with the New Processes I group. He contributed with more than 30 peer-reviewed articles in the fields of advanced microscopy, material science, and thin-film chalcopyrite solar cells.

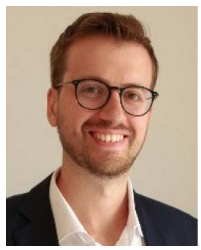

Alberto Lomuscio received the Ph.D. degree in physics from the University of Luxembourg, Esch-sur-Alzette, Luxembourg, on optical defect spectroscopy in $CuInS_2$ thin-films and solar cells, in 2020.

He then joined the AVANCIS R&D Center, Munich, Germany, as a Research and Development Engineer with the New Processes I group. Since 2015, he has been working in thin-film chalcopyrite solar cells with more than 20 publications and conference contributions. His current activities are focused on back contact and CIGSSe absorber development.

Detlef Helmecke received the graduate degree from the Mining Academy, Freiberg, Germany, in 1979 followed by different technical and electrical vocational trainings. He has intensive experience in CIGSSe thin-film technology for more than 15 years. In 2008, he joined AVANCIS R&D Center, Munich, Germany, where he is currently holding the position of a Senior Development Technician with the New Processes I group. He is responsible for the precursor deposition process including the plant maintenance as well as process control and development. He has previous industry experience with Infineon Technologies AG, Laser Components GmbH, and others.

Christian Schubbert received the Ph.D. degree in physics from the University of Oldenburg, Oldenburg, Germany, on the study of energy yield influencing properties of CIGSSe, in 2016.

He worked on thin-film solar cells for more than 14 years and joined Avancis R&D Center, Munich, Germany, in 2011 first as a Ph.D. student and currently working with the characterization group as a Specialist on IV characterization, device simulation, and stability testing. He has authored or coauthored more than 15 publications.

Souhaib Oueslati received the Ph.D. degree in physics from the University of Tunis EL-Manar, Tunis, Tunisia, on electrical characterization and modeling of kesterite-based solar cell in cooperation with imec, Belgium, in 2015.

He then joined the Crystalsol OÜ R&D Center, Tallinn, Estonia, as a Development Engineer before being awarded a Postdoctoral Researcher Grant in 2017 followed by another research grant in 2020 with Tallinn University of Technology, Estonia working on Kesterite monograins. He then joined the AVANCIS R&D Center, Munich, Germany, as a Development Engineer with the New Processes I group. Since 2013, he has been working in solar cells with more than 20 publications and conference contributions.

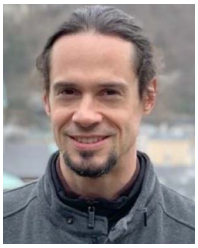

Matej Hála received the Ph.D. degree in engineering physics from Polytechnique Montréal, Montreal, QC, Canada, on the characterization of high-power impulse magnetron sputtering discharges, in 2011.

After a Postdoctoral and Research Associate positions with the Laboratory for Photovoltaics, University of Luxembourg, he joined the AVANCIS R&D Center, Munich, Germany, in 2016. As an R&D Project Leader, he focuses on development, upscaling, and management of vacuum-based coating processes. He contributed to 14 reviewed articles and nine conference papers.

Julian Röder received the M.Sc. degree in energy science from the University of Bayreuth, Bayreuth, Germany, in 2018.

During the study, his focus was already on energy conversion and energy production processes. Since 2018, he has been with AVANCIS R&D Center, Munich, Germany, first generally supporting all production processes before he was specializing to patterning and contacting processes. He contributed to three conference presentation and papers so far.

Florian Giesl received the M.Sc. degree in physics from the University of Regensburg, Regensburg, Germany, on commensurability oscillations in surface states of a topological insulator, in 2017.

In 2018, he joined the R&D Department, AVANCIS GmbH, Munich, Germany, for working toward the Ph.D. degree and has been a Development Engineer with the New Process I group since 2021. The current focus of his work lies on device simulations and statistical analysis of absorber compositions. He contributed to three peer-reviewed publications in the field of chalcopyrite solar cells.

Thomas Dalibor (Member, IEEE) received the Ph.D. degree in physics from the University of Erlangen-Nürnberg, Erlangen, Germany, on the electrical and optical characterization of silicon carbide, in 2002.

Initially, he worked in the development of high-power semiconductors as well as in the development and production of CMOS devices. Since 2008, he has been with AVANCIS GmbH, Munich, Germany. As the Director CTO, he is heading the AVANCIS' R&D Center in Munich. He has authored or coauthored more than 90 papers and publications as well as coauthored a book chapter for the *Landolt-Börnstein Series*. Since 2014, he has been a Member of the Scientific Committee of the European Photovoltaic Solar Energy Conference and Exhibition.